Electrochemistry Very Important Paper

How to cite: *Angew. Chem. Int. Ed.* **2021**, *60*, 19169–19175
International Edition: doi.org/10.1002/anie.202103102
German Edition: doi.org/10.1002/ange.202103102

Identifying Structure–Selectivity Correlations in the Electrochemical Reduction of CO_2: A Comparison of Well-Ordered Atomically Clean and Chemically Etched Copper Single-Crystal Surfaces

*Fabian Scholten, Khanh-Ly C. Nguyen, Jared P. Bruce, Markus Heyde, and Beatriz Roldan Cuenya**

Abstract: *The identification of the active sites for the electrochemical reduction of CO_2 (CO_2RR) to specific chemical products is elusive, owing in part to insufficient data gathered on clean and atomically well-ordered electrode surfaces. Here, ultrahigh vacuum based preparation methods and surface science characterization techniques are used with gas chromatography to demonstrate that subtle changes in the preparation of well-oriented Cu(100) and Cu(111) single-crystal surfaces drastically affect their CO_2RR selectivity. Copper single crystals with clean, flat, and atomically ordered surfaces are predicted to yield hydrocarbons; however, these were found experimentally to favor the production of H_2. Only when roughness and defects are introduced, for example by electrochemical etching or a plasma treatment, are significant amounts of hydrocarbons generated. These results show that structural and morphological effects are the key factors determining the catalytic selectivity of CO_2RR.*

Introduction

The electrocatalytic conversion of carbon dioxide (CO_2RR) into valuable hydrocarbons, alcohols as well as carbon monoxide has gained significant attention within recent years as a promising technology to close the carbon cycle and to build a sustainable and clean economy.

A remaining challenge is that even though advances on the engineering side of the field have been made pushing the obtained faradaic efficiencies higher than 80% for some of the desired C_2 hydrocarbons,[1] fundamental knowledge on how the conversion proceeds at the atomic scale remains up to debate.[2–6] The CO_2RR is a complex reaction whose selectivity depends on many factors such as the pH,[7,8] chemical state,[9–13] electrolyte composition,[14–16] surface coverage[17–21] and binding strength of the reaction intermediates.[14,20,22,23] Theoretical and experimental studies attempting to understand the CO_2RR mechanisms have mainly focused on Cu(hkl) single crystal surfaces.[3,6,18,20,24–26] Cu(100) and Cu(111) have garnered particular interest due to significantly different CO_2RR selectivity with highly desirable C_2 products favoured on the Cu(100) surfaces.[18,25,26]

By understanding the facet-dependent selectivity of model single crystal surfaces, results obtained on polycrystalline and/or oxide derived systems could be better understood as a function of the presence of specific facets and/or adsorption sites.[10,18,23,24] This would also allow us to decouple the influence of oxides present during the reaction from structural surface properties.[26,27] Therefore, facetted nanoscale catalysts have been widely employed in the past.[21,28–31]

Much of the work present in the literature has been based upon foundational studies by Hori et. al.[18] that used mechanical and electrochemical polishing[18,26] methods to prepare the Cu(hkl) surfaces. On the other hand, theoretical calculations focused on pristine atomically ordered surfaces[24] that may not be suitable for the description of the more structurally and chemically complex real-world systems. For instance, in situ and operando spectroscopic and scanning probe microscopy studies showed that facetted surfaces change significantly under CO_2RR conditions.[26,27,29,32–34]

Although significant scientific effort has been dedicated to the understanding of the active motifs and sites in CO_2RR over Cu surfaces in order to tune their selectivity towards valuable hydrocarbons and fuels, numerous open questions still remain.[23,24,26,32,35] So far, mechanistic understanding has come from theoretical studies which still have numerous challenges to overcome in order to mimic realistic electrochemical reaction conditions. On the other hand, experimental studies on atomically well-defined model single crystal surfaces that would be analogues to the structures employed in the calculations are still largely missing.[18,26] By employing pristine atomically flat ultra-high vacuum (UHV)-prepared Cu(100) and Cu(111) surfaces for CO_2RR, the present work closes this gap.

Through a combination of microscopy and spectroscopy techniques, coupled to online gaseous product detection, it was possible to follow the evolution of the structure and chemical state of atomically flat Cu surfaces in the course of CO_2RR. In contrast to prior theoretical predictions, such surfaces do not exhibit a high hydrocarbon selectivity, but instead, drastically favour hydrogen evolution over CO_2RR. The controlled introduction of defects by in situ UHV and ex

[*] F. Scholten, K.-L. C. Nguyen, J. P. Bruce, M. Heyde, B. Roldan Cuenya
Interface Science Department
Fritz-Haber Institute of the Max Planck Society
14195 Berlin (Germany)
E-mail: Roldan@fhi-berlin.mpg.de

Supporting information and the ORCID identification number(s) for the author(s) of this article can be found under: https://doi.org/10.1002/anie.202103102.

situ pre-treatments was needed to shift the selectivity towards hydrocarbons up to the values reported for electrochemically polished single crystal surfaces[18,25,26] Furthermore, by using CO as a probe molecule, the CO-binding strength on the differently prepared surfaces was found to correlate to the hydrocarbon selectivity.[22]

Results

The morphology of all samples prepared in UHV by a combination of Ar sputtering and annealing prior to any further pre-treatment before the electrochemical testing was monitored via UHV scanning tunneling microscopy (STM) and ex situ atomic force microscopy (AFM). Details on the sample preparation workflow and electrochemical set-up can be found in the Supporting Information, Figures S1 and S2. STM measurements at room temperature in UHV yielded atomically resolved images within large terraces as shown in Figure 1 a (inset), 2a (inset) and Figure S3 for the Cu(100) and Cu(111) surfaces, respectively. Ex situ AFM images also confirmed the existence of large terraces separated by well-defined step edges or bunches, Figures 1,2 (a). X-ray photoelectron spectroscopy (XPS) data confirmed the cleanliness of these UHV prepared and sputtered surfaces, showing only metallic Cu without any additional elements present, Figures S4, S5 (a,b) and S6 (a,b).

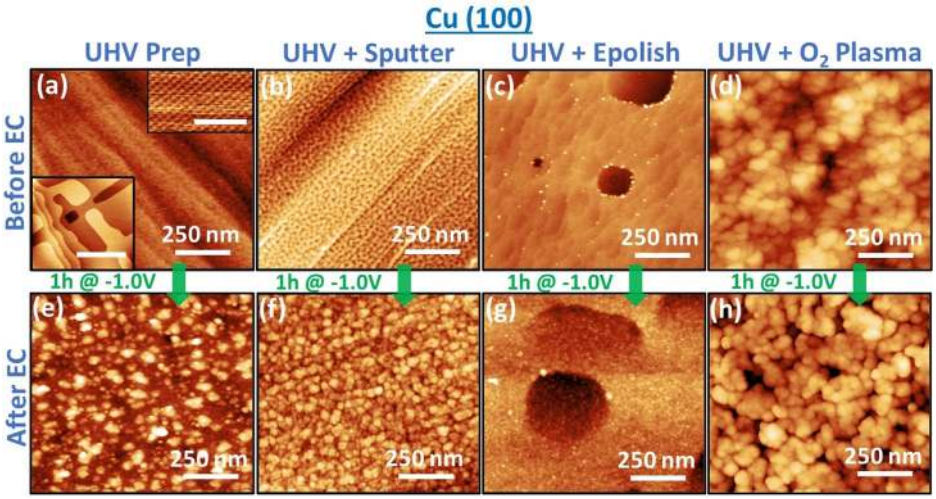

Figure 1. Ex situ AFM images of a Cu(100) single crystal surface acquired in air after different pre-treatments before (a–d) and after 1 h of CO_2RR at −1.0 V vs. RHE in 0.1 M $KHCO_3$ (e–h). The insets in (a) show room temperature UHV-STM images from large terraces (100 nm scale bar) and an atomically resolved area (2 nm scalebar). The color scale of the AFM images goes from dark to bright; a) 0–4 nm, b) 0–5 nm, c),f),g) 0–12 nm, e) 0–20 nm and d),h) 0–50 nm.

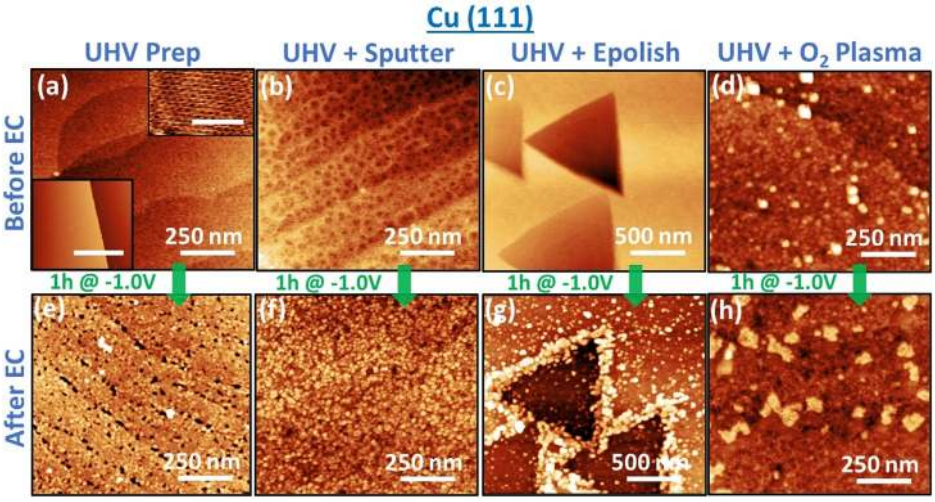

Figure 2. Ex situ AFM images of a Cu(111) single crystal surface acquired in air after different pre-treatments before (a–d) and after 1 h of CO_2RR at −1.0 V vs. RHE in 0.1 M $KHCO_3$ (e–h). The insets in (a) show room temperature UHV-STM images from large terraces (100 nm scale bar) and an atomically resolved area (2 nm scale bar). The color scale for the AFM images goes from dark to bright; a) 0–2 nm, b) 0–4, c)–f),h) 0–12 nm, g) 0–14 nm.

Electropolishing and ex situ oxygen plasma treatments have been used to increase the number of defects and the overall roughness of the UHV-prepared samples.[9] The corresponding AFM images are displayed in Figure 1 and Figure 2 (c-d) for the Cu(100) and Cu(111) single crystals, respectively. Depending on the crystal orientation, the different pre-treatments affect the surface differently. Sputtering of the Cu(100) surface yields small holes (ca. 2 nm depth), while a network-like structure with larger holes (ca. 5 nm depth) is found on the Cu(111) surface. In the electropolished samples, the well-defined step edges/bunches observable for the UHV-sputtered samples are lost, which is accompanied by the appearance of square or triangular- shaped etch pits, depending on the surface orientation. These structures are linked to oxygen etching when employing high anodic potentials.[18] Interestingly, the overall roughness as probed by AFM is rather similar for the pristine UHV, the UHV-sputtered and the electropolished samples, even though the local morphology and type of defects observed are clearly distinct (Table S1).

Pre-treatment of the Cu surface with oxygen plasma shows significantly different restructuring as compared to the other treatments. Oxidation to Cu_2O by the O_2-plasma is

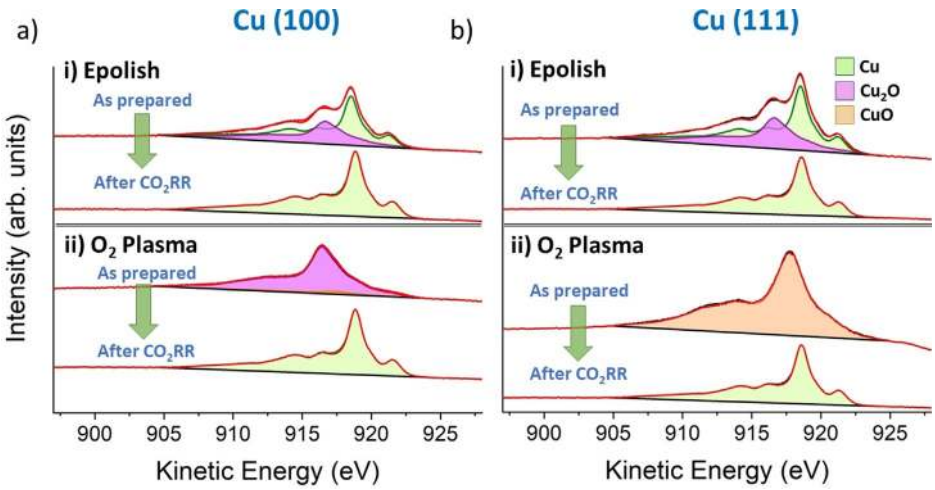

Figure 3. Quasi in situ Cu LMM XPS data obtained before and after 1 h of CO_2RR at −1.0 V vs. RHE in 0.1 M $KHCO_3$ for a) Cu(100) and b) Cu(111). The data are fitted by linear combination using reference spectra measured for Cu, Cu_2O and CuO.

revealed by the XPS data, Figure 3, Figure S4 and S5, and AFM shows the roughening of the Cu(100) surface accompanied by the presence of agglomerated nanoparticle-like structures (Table. S1). A smaller roughness and less plasma-driven restructuring is observed for Cu(111) (Table S1), which is assigned to the difference in oxidation to CuO that the sample undergoes. It should be noted that conducting atomically resolved STM imaging in UHV on electropolished and other electrochemically treated samples has been attempted but found very challenging due to the presence of residual carbonaceous species. Furthermore, any attempt to subsequently clean these surfaces might lead to an undesired change of the surface structure. Nonetheless, ex situ AFM images of the different surfaces after exposure to the CO_2RR conditions for 1 h in 0.1 M $KHCO_3$ show the formation of particulate aggregates on the surface of all samples. Surprisingly, the initial surface features like step edges showing holes alongside them (Figure 2e), or the etch pits formed through some of the pre-treatments (covered by particles in the case of the Cu(111) surface, Figure 2g), still persist through the CO_2 electrolysis. The particles and agglomerates observable on all surfaces after electrochemistry are either Cu or C species as shown by XPS, which only detects carbon and oxygen in addition to Cu after electrochemistry, Figure S7.

Quasi in situ XPS Cu LMM (Figure 3) and O-1s (Figure S5) spectra acquired after 1 h CO_2RR reveal that, regardless of the initial pre-treatment and as-prepared oxidation state on our relatively smooth surfaces (ca. 37% Cu_2O + 63% Cu for both electropolished surfaces, 93% Cu_2O + 7% CuO for plasma-treated Cu(100) and 100% CuO for plasma-treated Cu(111), Table S2), copper is in its metallic state after CO_2RR, in agreement with prior literature reports.[11,27,36–38] This finding rules out oxidation state effects or the presence of subsurface oxygen in the single crystals as responsible for the different selectivity trends displayed below.

Carbon monoxide (CO) is an important intermediate in the CO_2RR reaction and is used here to probe its binding energy to the different initial Cu surfaces using temperature programmed desorption. Such measurements have been previously proven highly valuable to gain insight on polycrystalline Cu surfaces within the framework of CO_2 electroreduction,[14,22] or were applied in isolation[39] to well-defined single crystal surfaces but, never in combination as implemented here. A summary of the results for the differently prepared samples is shown in Figure 4 and the complete datasets in Figures S8 and S9. Table S3 summarizes the different CO binding sites on the distinct surfaces together with the binding energies extracted from the Redhead method[40] assuming a first order desorption process.

In Figure 4, for high CO exposures (1 L), the binding strength of CO on the pristine UHV-prepared Cu(100) is higher than on the Cu(111) surface (black dashed line for the highest desorption temperature peak), which is in agreement with current literature.[41] The strongest binding sites can be observed for the lowest CO dosing of 0.01 L, with 154 K for Cu(100) and 147 K for Cu(111). Following the Redhead model, CO desorption activation energies of 39.5 kJ mol^{-1} and 36.2 kJ mol^{-1} were obtained, respectively, Table S3. These peaks have been attributed to CO sitting linearly on top of terrace sites, with the C atom bound to Cu.[41,42] With increasing CO coverage, an additional desorption peak at lower temperature is detected on each surface. On Cu(111) this new desorption feature appears at 113 K and is sharper than the one detected on Cu(100) at 121 K. These peaks, that are observed at high CO dosage when the saturation of the

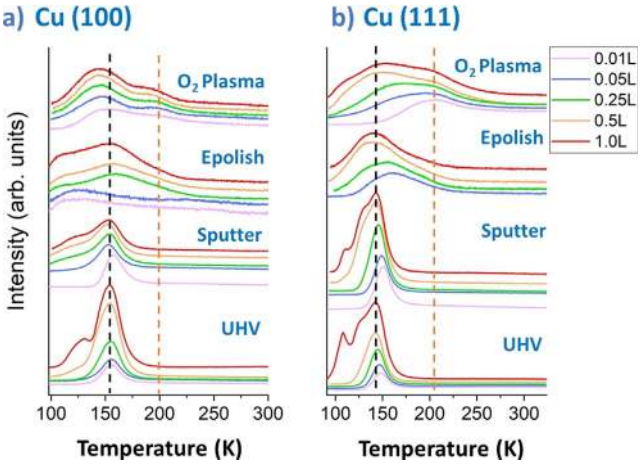

Figure 4. CO temperature programmed desorption (TPD) data acquired on differently pre-treated Cu(100) (a) and Cu(111) (b) single-crystal surfaces before CO_2RR. A heating rate of 2 K s^{-1} was used, and a maximum background dosing of CO of 1 L for all cases.

surface is expected and multilayer adsorption takes place, as also seen by the scalability of the peaks at higher dosing (Figure S8 and S9), are affected by the interaction of CO molecules with each other, which results in a weaker binding to the Cu surface.[39,41,43]

Similar features and line shapes can be observed for sputtered surfaces, indicating that the short-range atomic order of the surface remains similar, even though AFM shows these surfaces to be disturbed on a mesoscopic scale. It is clear however that the mild sputtering of a flat (pre-annealed) Cu surface affects the CO binding properties, as slightly higher desorption temperatures were obtained for the lowest CO dosing (0.01 L) that probed the strongest binding sites, with 157 K for Cu(100) and 150 K for Cu(111). Also the lower temperature desorption features for Cu(100) are found to be broader and less defined, indicating a more disordered CO saturation and multilayer coverage. Also it appears that the CO surface-saturation is reached at lower CO exposures on the sputtered samples.

For the electropolished surfaces, the observed CO desorption peaks are significantly broader for all coverages and the peak maximum for lower coverages (e.g. 0.05 L for Cu(111)) is shifted to higher desorption temperatures of 163 K for Cu(111), indicating a stronger CO binding with respect to the UHV-prepared surfaces. It was challenging, however, to acquire TPD data for these surfaces at lower CO coverages, likely due to residual contamination arising from the electrochemical pre-treatment. Nevertheless, the trend of stronger binding is clearly visible for both surfaces, especially for the highest dosing cases of 1.0 L, as shoulder peaks at temperatures as high as 185 K for Cu(100) and 198 K for Cu(111) were additionally present.

The O_2-plasma pre-treated samples clearly show the strongest binding sites, with peaks at 199 K and 206 K for Cu(100) and Cu(111) at 0.01 L, corresponding to desorption activation energies of 51.4 an 53.3 kJ mol^{-1}. This finding suggests the presence of a large amount of high-index stepped sites as well as defects within the atomic lattice.[22,41–43] In agreement to what has been previously observed on polycrystalline samples, the strong CO-binding sites are even more dominantly present for oxide-derived and O_2-plasma treated samples[14,22] as compared to the electrochemically etched ones. The latter reveals that the sample pre-treatment has in fact a strong effect on the defect density and morphological features formed on Cu surfaces that are expected to significantly affect the stability of CO and CO-like intermediates during CO_2RR, which will be discussed later.

The electrochemical CO_2RR activity and selectivity of the differently pre-treated samples is shown in Figures 5 and 6. Additional chronoamperometric curves are displayed in Figure S10 and the electrochemical surface area (ECSA) in Table S4. Interestingly, the ECSA data acquired after 1 h of CO_2RR, Figure S11, yielded a similar roughness for all samples with the exception of the plasma-treated samples and to a lesser degree the electropolished ones (Table S4), which were found to be rougher. This is consistent with our AFM analysis finding that revealed that all UHV-prepared samples were widely flat, even after electrochemistry.

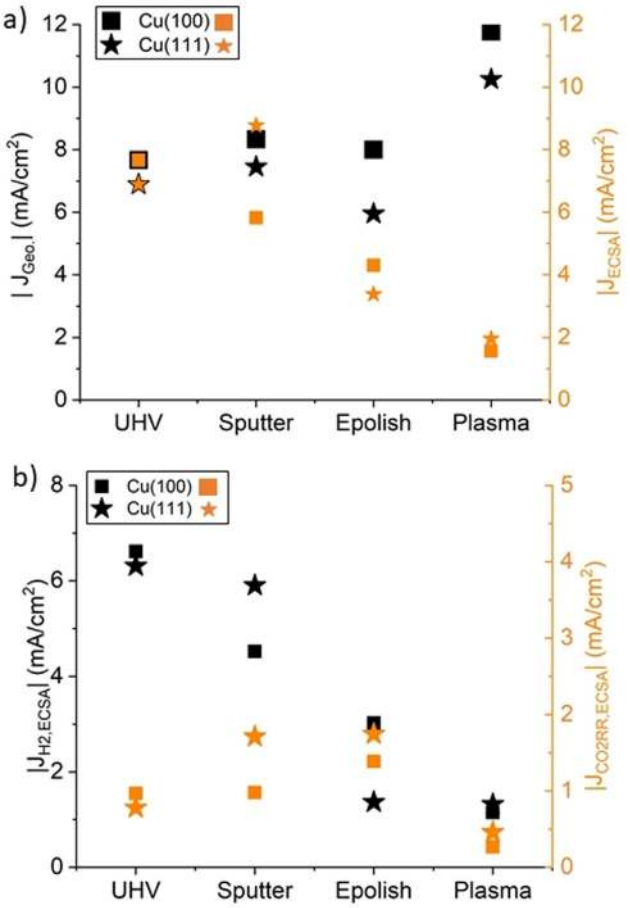

Figure 5. a) Total geometric- (left) and ECSA-normalized (right) current densities and b) partial ECSA-normalized current densities for H_2 (left) and the combined CO_2RR products (right) acquired on differently prepared Cu(100) and Cu(111) single crystal surfaces during 1 h of CO_2RR at −1.0 V vs. RHE in 0.1 M $KHCO_3$.

Apart from the O_2-plasma pre-treated samples, no drastic changes in the total geometric current density were observed for Cu(100) or Cu(111), Figure 5(a) and Table S5. However, a general apparent decrease in the activity is observed for the electropolished and O_2-plasma treated samples when the ECSA is used for the normalization of the current densities. This decrease appears to be associated with a lower partial current density for H_2, as can be seen in Figure 5(b). ECSA-normalized partial current densities for the remaining products are shown in Figure S12.

As can be seen in Figure 6, the pristine well-ordered clean surfaces do not exhibit a high amount of hydrocarbon generation unlike what is expected from reports in the literature on similar oriented surfaces,[2,18,24] but generate hydrogen as major product. The exception to this is the surface obtained after the electropolishing pre-treatment that results in a selectivity in good agreement with previous reports applying similar treatments.[18,25,26]

While the addition of surface defects via Ar-sputtering results in an increased hydrocarbon generation as compared to the pristine UHV-prepared samples, the C_{2+} selectivity is marginally improved (5–8%) for both crystal orientations.

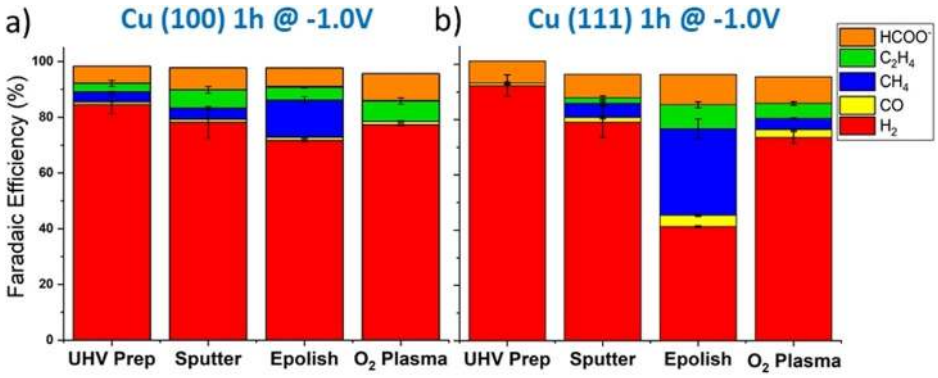

Figure 6. Distribution of the main CO_2RR products (Faradaic efficiency) for differently prepared Cu(100) (a) and Cu(111) (b) single crystal surfaces obtained after 1 h of CO_2RR at −1.0 V vs. RHE in 0.1 M $KHCO_3$. The data are averaged over two experiments with three injections each.

Nevertheless, some differences in the selectivity of both surfaces can be observed, with Cu(100) favoring the generation of ethylene and Cu(111) that of methane.[25] In accordance with prior work on oxide-derived catalysts, the O_2-plasma treated samples exhibit a higher C_2 hydrocarbon selectivity that is independent of the surface orientation.[9] This observation supports the idea that the oxide-derived effect is not linked to specific surface terrace orientation but is instead linked to the presence of specific morphological defect sites.[23] These findings are also reflected in the trend depicted in Figure S13, where a correlation between the strength of the binding of CO to the different Cu surfaces and the selectivity for C_2 products is presented. The data shown correspond to the CO desorption activation energies obtained by TPD on the differently pre-treated Cu surfaces for the lowest-CO coverages that could be detected. Such low CO dosings were selected as reference to probe the strongest binding sites that are first populated. Interestingly, the samples displaying the strongest CO binding sites (O_2-plasma pre-treated) were also the ones in which the C–C coupling was favored. It should be however noted that this is only a qualitative trend and that further work is still needed to fully understand the trends observed.

Alcohols could only be detected in trace amounts (< 1 %) for the electropolished and plasma treated samples. Contamination and impurities are known to stifle the CO_2RR performance for Cu-based catalysts,[44] however, the XPS data only show Cu, C and O to be present after electrochemistry (Figure S7), reassuring that residual contamination is not driving the differences observed in the selectivity presented here. Similarly, no copper oxide species were found to remain on these surfaces after CO_2RR according to XPS.

Discussion

Our work on clean atomically ordered Cu single crystal surfaces intends to provide a benchmark for the field of CO_2RR with respect to the expected structure-selectivity trends for contaminant-free samples with a low density of defects. On these UHV-prepared Cu surfaces, our experimental data clearly reveal that CO_2RR selectivity data extracted from electropolished, differently oriented Cu single crystal surfaces may not be the ideal proxy for theoretical predictions on these surfaces. As it is demonstrated here, even ideal UHV-prepared surfaces experience significant structural changes under CO_2RR, as was already previously suggested.[45] In fact, and regardless of the surface orientation, we revealed that the least-defective Cu surfaces prepared (pristine UHV-treated samples) are not highly selective for hydrocarbons, specially C_{2+} products, but for the parasitic hydrogen evolution reaction. It is only when defects are purposely introduced to the flat atomically ordered pristine Cu surfaces that we start to see the generation of hydrocarbons up to the values reported in the literature corresponding to the electropolished samples with a disordered and defective surface, as indicated by our AFM and TPD analysis.[18,25] In agreement with our findings, the possibility of introducing defects and other active structural motifs upon electropolishing Cu single crystal surfaces has also been previously described based on cyclic voltammetry experiments.[46]

Many theoretical studies[24,47] have been successful at reproducing the high hydrocarbon yields obtained experimentally on electropolished surfaces that we now demonstrate are far from atomically ordered and structurally ideal. In clear contrast, our present experimental work indicates that theoretical calculations carried out on pristine (defect-free) Cu surfaces should show a preferred H_2 yield, which does not seem to be the case in prior theoretical reports. We hope that the present findings stimulate further development of theoretical models, including more defective surfaces that might help us solve this puzzle.

Moreover, we could demonstrate that the presence of stronger CO bindings sites increases the amount of hydrocarbons generated. Samples containing a higher amount of defect sites and high index facets, as probed by CO TPD, were also found to display a higher hydrocarbon yield, thus favoring CO_2RR over HER. This is in agreement to prior reports on polycrystalline Cu featuring a higher ethylene selectivity when strong CO binding sites were available.[14,22] Such sites encompass defects on the terraces, steps and high index facets which mainly evolve when the pristine samples are exposed to harsh pre-treatments such as electropolishing or an oxidation and subsequent electrochemical reduction under CO_2 reaction conditions. Thus, it appears that the catalytic reduction of CO_2 from its initial activation on the surface towards the crucial C–C coupling step takes place at undercoordinated surface atoms (defects) and step edges.[24,25,35]

Previously, the high selectivity for methane of electropolished non-oxide-derived Cu surfaces, has been fundamentally ascribed to the presence of an specific surface facet, such

as Cu(111), and that of ethylene to Cu(100).[21,24,25] Our experiments reveal that when ideal, both of these atomically ordered surfaces mainly produce H_2, and that the presence of specific defects (undercoordinated sites, steps) is more important than large terraces with a specific surface orientation. Similarly, the performance of nanostructured materials, which has been interpreted within the same structural framework, should be now re-evaluated.[21,31]

It should be also highlighted that prior literature assumptions have been based on experimental data obtained on "model" electropolished Cu single crystals which are, as demonstrated here, drastically different from pristine surfaces. In particular, the latter are almost inert for CO_2RR. Thus, more emphasis should be put on the presence of specific step, defective and undercoordinated sites and their impact in nanostructured catalysts to understand their catalytic performance.

Our results suggest that large low index terraces do not facilitate the reduction of CO_2, but favor HER, and that hydrocarbon products are only detected upon introducing defects, step edges/bunches and high index facets.[24,47] This explanation is in line with a possible correlation obtained between the ratio of C_2/C_1 products and the strength of the CO binding for the lowest detectable CO coverages (strongest binding sites) on the differently pre-treated single crystal surfaces before electrochemistry, Figure S12. We have also demonstrated experimentally that the structure of the distinct single crystal surfaces investigated does not remain static under CO_2RR. Thus, this evolution could also affect the strength of the CO binding that we can only probe experimentally (CO-TPD in UHV) on the clean samples before reaction. Nonetheless, and despite these transformations, it is clear from Figure 6 that the initial pre-treatment and structure of the Cu surface has a very strong effect in the final product selectivity. Therefore, we consider that the apparent correlation observed between the CO binding strength to the pristine Cu surfaces and the C_2/C_1 product selectivity will be a valuable piece of information for theorists calculating possible reaction pathways over Cu surfaces, given that they also do not generally consider in their complex calculations reaction-induced surface reconstructions.

A possible reason for the observed trends could be that the initial CO_2 activation and consequent reduction to CO is not achieved on pristine low index surfaces due to a weak binding of CO_2 on these. We hope that our experimental study will inspire further theoretical work in this direction.

Since the amount of hydrocarbons seen for the electropolished samples is the highest, this suggests that the overall roughness (which was the highest for the O_2-plasma treated sample) cannot be solely accountable for the selectivity trends observed.[9,26] Taking into account our quasi in situ XPS results (Figure 3) demonstrating that all flat surfaces are metallic after potentiotstatic CO_2RR conditions (1 h CO_2RR),[11,26,48,49] the specific surface structure and presence of defects and steps seems to play the main role in determining whether the surface is active for CO_2RR or HER. Furthermore, the enhanced performance for ethylene widely reported in the literature for Cu(100) surfaces must be revisited, since such selectivity may only be obtained when highly defective Cu(100) surfaces are considered, including the rough surfaces obtained after the electropolishing treatments.

This is in agreement with our recent finding on Cu(100) surfaces exposed to pulse electrolysis conditions, where we could demonstrate that defects and higher index facets that are present as a consequence of the electropolishing pretreatment and the electrochemical reduction of Cu_xO species affect the ethylene yields.[26] In the former work however, the Cu^I species formed through anodic surface pulsing were found to favor the formation of ethanol, which is not observed here on the atomically flat reduced Cu surfaces investigated under constant negative applied potential (−1.0 V).

Conclusion

By combining the benefits of UHV preparation methods and various pre-treatments with detailed morphological characterization, a drastic impact of the surface structure on the selectivity for CO_2RR or HER of low-index Cu single crystal surfaces was revealed. While pristine surfaces consisting of large atomically ordered low index facets are found to be almost inert for the reduction of CO_2, defective and higher index surfaces lead to the generation of hydrocarbons through CO_2RR. Interestingly, the yield of C_2/C_1 products was found to be higher for the surfaces exhibiting a higher CO binding strength.

Since theoretical calculations are majorly based on modelling the CO_2RR on pristine surfaces, our findings highlight the importance of considering different types of defects in their models. The present study emphasizes that, unlike previously thought, pristine atomically ordered low index facets such as Cu(100) are not the active sites for CO_2RR, including not yielding significant amounts of C_2H_4 at the expense of hydrogen, until surface pre-treatments leading to the formation of steps and other surface defects are undertaken. Such defects, created for example during the conventional electropolishing treatments or during pre-oxidation-reduction routines, and are in fact responsible for the desirable catalytic selectivity towards hydrocarbons.

Acknowledgements

This work was supported by the European Research Council under grant ERC-OPERANDOCAT (ERC-725915) and the deutsche Forschungsgemeinschaft (DFG) under the grant SFB1316, subproject B1 and Germany's Excellence Strategy—EXC 2008–390540038—UniSysCat. We thank Dr. Nikolai Berdunov for excellent technical support in the maintenance of the UHV system used. Open access funding enabled and organized by Projekt DEAL.

Conflict of Interest

The authors declare no conflict of interest.

Keywords: carbon dioxide · copper · electrochemistry · electro-reduction · single crystals

[1] M. G. Kibria, C. T. Dinh, A. Seifitokaldani, P. De Luna, T. Burdyny, R. Quintero-Bermudez, M. B. Ross, O. S. Bushuyev, F. P. García de Arquer, P. Yang, D. Sinton, E. H. Sargent, *Adv. Mater.* **2018**, *30*, 1 – 7.

[2] A. J. Garza, A. T. Bell, M. Head-Gordon, *ACS Catal.* **2018**, *8*, 1490 – 1499.

[3] T. K. Todorova, M. W. Schreiber, M. Fontecave, *ACS Catal.* **2020**, *10*, 1754 – 1768.

[4] K. J. P. Schouten, Y. Kwon, C. J. M. Van Der Ham, Z. Qin, M. T. M. Koper, *Chem. Sci.* **2011**, *2*, 1902 – 1909.

[5] A. A. Peterson, F. Abild-Pedersen, F. Studt, J. Rossmeisl, J. K. Nørskov, *Energy Environ. Sci.* **2010**, *3*, 1311 – 1315.

[6] F. Calle-Vallejo, M. T. M. Koper, *Angew. Chem. Int. Ed.* **2013**, *52*, 7282 – 7285; *Angew. Chem.* **2013**, *125*, 7423 – 7426.

[7] A. S. Varela, M. Kroschel, T. Reier, P. Strasser, *Catal. Today* **2016**, *260*, 8 – 13.

[8] R. Kortlever, J. Shen, K. J. P. Schouten, F. Calle-Vallejo, M. T. M. Koper, *J. Phys. Chem. Lett.* **2015**, *6*, 4073 – 4082.

[9] H. Mistry, A. S. Varela, C. S. Bonifacio, I. Zegkinoglou, I. Sinev, Y.-W. Choi, K. Kisslinger, E. A. Stach, J. C. Yang, P. Strasser, B. R. Cuenya, *Nat. Commun.* **2016**, *7*, 12123.

[10] P. De Luna, R. Quintero-Bermudez, C. T. DInh, M. B. Ross, O. S. Bushuyev, P. Todorović, T. Regier, S. O. Kelley, P. Yang, E. H. Sargent, *Nat. Catal.* **2018**, *1*, 103 – 110.

[11] F. Scholten, I. Sinev, M. Bernal, B. Roldan Cuenya, *ACS Catal.* **2019**, *9*, 5496 – 5502.

[12] H. Xiao, W. A. Goddard, T. Cheng, Y. Liu, *Proc. Natl. Acad. Sci. USA* **2017**, *114*, 6685 – 6688.

[13] M. Fields, X. Hong, J. K. Nørskov, K. Chan, *J. Phys. Chem. C* **2018**, *122*, 16209 – 16215.

[14] D. Gao, I. T. McCrum, S. Deo, Y. W. Choi, F. Scholten, W. Wan, J. G. Chen, M. J. Janik, B. Roldan Cuenya, *ACS Catal.* **2018**, *8*, 10012 – 10020.

[15] A. S. Varela, W. Ju, T. Reier, P. Strasser, *ACS Catal.* **2016**, *6*, 2136 – 2144.

[16] J. Resasco, L. D. Chen, E. Clark, C. Tsai, C. Hahn, T. F. Jaramillo, K. Chan, A. T. Bell, *J. Am. Chem. Soc.* **2017**, *139*, 11277 – 11287.

[17] D. Gao, F. Scholten, B. Roldan Cuenya, *ACS Catal.* **2017**, *7*, 5112 – 5120.

[18] Y. Huang, A. D. Handoko, P. Hirunsit, B. S. Yeo, *ACS Catal.* **2017**, *7*, 1749 – 1756.

[19] J. Li, Z. Wang, C. McCallum, Y. Xu, F. Li, Y. Wang, C. M. Gabardo, C. T. Dinh, T. T. Zhuang, L. Wang, J. Y. Howe, Y. Ren, E. H. Sargent, D. Sinton, *Nat. Catal.* **2019**, *2*, 1124 – 1131.

[20] R. B. Sandberg, J. H. Montoya, K. Chan, J. K. Nørskov, *Surf. Sci.* **2016**, *654*, 56 – 62.

[21] Y. Wang, Z. Wang, C. T. Dinh, J. Li, A. Ozden, M. Golam Kibria, A. Seifitokaldani, C. S. Tan, C. M. Gabardo, M. Luo, H. Zhou, F. Li, Y. Lum, C. McCallum, Y. Xu, M. Liu, A. Proppe, A. Johnston, P. Todorovic, T. T. Zhuang, D. Sinton, S. O. Kelley, E. H. Sargent, *Nat. Catal.* **2020**, *3*, 98 – 106.

[22] A. Verdaguer-Casadevall, C. W. Li, T. P. Johansson, S. B. Scott, J. T. McKeown, M. Kumar, I. E. L. Stephens, M. W. Kanan, I. Chorkendorff, *J. Am. Chem. Soc.* **2015**, *137*, 9808 – 9811.

[23] Y. Lum, J. W. Ager, *Nat. Catal.* **2019**, *2*, 86 – 93.

[24] A. Bagger, W. Ju, A. S. Varela, P. Strasser, J. Rossmeisl, *ACS Catal.* **2019**, *9*, 7894 – 7899.

[25] Y. Hori, I. Takahashi, O. Koga, N. Hoshi, *J. Mol. Catal. A Chem.* **2003**, *199*, 39 – 47.

[26] R. M. Arán-Ais, F. Scholten, S. Kunze, R. Rizo, B. Roldan Cuenya, *Nat. Energy* **2020**, *5*, 317 – 325.

[27] T. H. Phan, K. Banjac, F. P. Cometto, F. Dattila, R. García-Muelas, S. J. Raaijman, C. Ye, M. T. M. Koper, N. López, M. Lingenfelder, *Nano Lett.* **2021**, *21*, 2059—2065.

[28] T. Möller, F. Scholten, T. N. Thanh, I. Sinev, J. Timoshenko, X. Wang, Z. Jovanov, M. Gliech, B. Roldan Cuenya, A. S. Varela, P. Strasser, *Angew. Chem. Int. Ed.* **2020**, *59*, 17974 – 17983; *Angew. Chem.* **2020**, *132*, 18130 – 18139.

[29] P. Grosse, D. Gao, F. Scholten, I. Sinev, H. Mistry, B. Roldan Cuenya, *Angew. Chem. Int. Ed.* **2018**, *57*, 6192 – 6197; *Angew. Chem.* **2018**, *130*, 6300 – 6305.

[30] G. L. De Gregorio, T. Burdyny, A. Loiudice, P. Iyengar, W. A. Smith, R. Buonsanti, *ACS Catal.* **2020**, *10*, 4854 – 4862.

[31] A. Loiudice, P. Lobaccaro, E. A. Kamali, T. Thao, B. H. Huang, J. W. Ager, R. Buonsanti, *Angew. Chem. Int. Ed.* **2016**, *55*, 5789 – 5792; *Angew. Chem.* **2016**, *128*, 5883 – 5886.

[32] G. H. Simon, C. S. Kley, B. Roldan Cuenya, *Angew. Chem. Int. Ed.* **2021**, *60*, 2561 – 2568; *Angew. Chem.* **2021**, *133*, 2591 – 2599.

[33] Y. G. Kim, J. H. Baricuatro, A. Javier, J. M. Gregoire, M. P. Soriaga, *Langmuir* **2014**, *30*, 15053 – 15056.

[34] S. H. Lee, J. C. Lin, M. Farmand, A. T. Landers, J. T. Feaster, J. E. Avilés Acosta, J. W. Beeman, Y. Ye, J. Yano, A. Mehta, R. C. Davis, T. F. Jaramillo, C. Hahn, W. S. Drisdell, *J. Am. Chem. Soc.* **2021**, *143*, 588 – 592.

[35] T. Cheng, H. Xiao, W. A. Goddard, *J. Am. Chem. Soc.* **2017**, *139*, 11642 – 11645.

[36] A. A. Permyakova, J. Herranz, M. El Kazzi, J. S. Diercks, M. Povia, L. R. Mangani, M. Horisberger, A. Pătru, T. J. Schmidt, *ChemPhysChem* **2019**, *20*, 3120 – 3127.

[37] S. B. Scott, T. V. Hogg, A. T. Landers, T. Maagaard, E. Bertheussen, J. C. Lin, R. C. Davis, J. W. Beeman, D. Higgins, W. S. Drisdell, C. Hahn, A. Mehta, B. Seger, T. F. Jaramillo, I. Chorkendorff, *ACS Energy Lett.* **2019**, *4*, 803 – 804.

[38] J. J. Velasco-Velez, R. V. Mom, L. E. Sandoval-Diaz, L. J. Falling, C. H. Chuang, D. Gao, T. E. Jones, Q. Zhu, R. Arrigo, B. Roldan Cuenya, A. Knop-Gericke, T. Lunkenbein, R. Schlögl, *ACS Energy Lett.* **2020**, *5*, 2106 – 2111.

[39] A. Kokalj, T. Makino, M. Okada, *J. Phys. Condens. Matter* **2017**, *29*, 194001.

[40] P. A. Redhead, *Vacuum* **1962**, *12*, 203 – 211.

[41] S. Vollmer, G. Witte, C. Wöll, *Catal. Lett.* **2001**, *77*, 97 – 101.

[42] M. Roiaz, L. Falivene, C. Rameshan, L. Cavallo, S. M. Kozlov, G. Rupprechter, *J. Phys. Chem. C* **2019**, *123*, 8112 – 8121.

[43] T. Makino, M. Okada, *Surf. Sci.* **2014**, *628*, 36 – 40.

[44] Y. Hori, H. Konishi, T. Futamura, A. Murata, O. Koga, H. Sakurai, K. Oguma, *Electrochim. Acta* **2005**, *50*, 5354 – 5369.

[45] W. Luo, X. Nie, M. J. Janik, A. Asthagiri, *ACS Catal.* **2016**, *6*, 219 – 229.

[46] A. K. Engstfeld, T. Maagaard, S. Horch, I. Chorkendorff, I. E. L. Stephens, *Chem. Eur. J.* **2018**, *24*, 17743 – 17755.

[47] X. Liu, J. Xiao, H. Peng, X. Hong, K. Chan, J. K. Nørskov, *Nat. Commun.* **2017**, *8*, 1 – 7.

[48] J. J. Velasco-Vélez, T. Jones, D. Gao, E. Carbonio, R. Arrigo, C. J. Hsu, Y. C. Huang, C. L. Dong, J. M. Chen, J. F. Lee, P. Strasser, B. Roldan Cuenya, R. Schlögl, A. Knop-Gericke, C. H. Chuang, *ACS Sustainable Chem. Eng.* **2019**, *7*, 1485 – 1492.

[49] Y. Lum, J. W. Ager, *Angew. Chem. Int. Ed.* **2018**, *57*, 551 – 554; *Angew. Chem.* **2018**, *130*, 560 – 563.

Manuscript received: March 2, 2021
Revised manuscript received: April 23, 2021
Accepted manuscript online: May 21, 2021
Version of record online: July 21, 2021

